

Modified Fresnel zone plates that produce sharp Gaussian focal spots

Qing Cao and Jürgen Jahns

Optische Nachrichtentechnik, FernUniversität Hagen, Universitätsstrasse 27/PRG, 58084 Hagen, Germany

Received January 14, 2003; revised manuscript received April 9, 2003; accepted April 10, 2003

A modified Fresnel zone plate that can produce an approximate Gaussian focal spot is proposed for the focusing and imaging of soft x rays and extreme ultraviolet radiation. The selection conditions for the positions and the widths of the concentric open rings are analytically presented. The focal spot size can be much smaller than the width of the narrowest open ring, and the sidelobes and the higher orders can be effectively suppressed. Through numerical experiments, we confirm that a Gaussian focal spot with a beam width of 7.7 nm can be produced by a modified Fresnel zone plate with a minimum structure size of 30 nm. © 2003 Optical Society of America

OCIS codes: 050.1970, 220.2560, 340.7440, 260.7200, 110.0110, 050.1940.

1. INTRODUCTION

The focusing and imaging of soft x rays and extreme ultraviolet radiation have many applications in physics and the life sciences, such as in high-resolution microscopy, spectroscopy, nanolithography, and telescope. Unfortunately, the refractive lens cannot be used for this kind of focusing because all solids are strongly absorbing in the spectral regions of soft x rays and extreme ultraviolet radiation. Traditional Fresnel zone plates (TFZPs) can be used for this kind of focusing.¹ However, the focal spot size of a TFZP is about the order of the width of the outermost half-zone,^{2–4} so its spatial resolution is limited in technology by the smallest structure (20–40 nm) that can be fabricated by lithography.^{5,6} This drawback was recently overcome by a novel diffractive optical element called a photon sieve,^{7–11} which consists of a large number of pinholes properly distributed over the Fresnel zones. It is well known that in a TFZP, each open ring has a net positive contribution to the field value at the desired focus. Similarly for a photon sieve, each pinhole has a net positive contribution to the field value at the desired focus. This collective behavior can greatly enhance the intensity at the desired focus and in fact is the cause of the focusing. However, it should be emphasized that the success (by which we mean the increase of spatial resolution, the suppression of sidelobes, and the suppression of higher orders) of photon sieves does not result from this aspect, but from the following three factors: First¹¹ is the use of large size for the whole element, though this point is not clearly mentioned in the initial work.⁷ The Rayleigh resolution formula tells us that larger optical elements lead to sharper focusing. The second factor⁷ is the use of smooth filtering for the population of pinholes. This kind of filtering can effectively suppress the sidelobes around the principal focus. The third factor¹⁰ is the use of different ratios $d:w$ for different pinholes, where d is the diameter of an individual pinhole and w is the width of the corresponding local half-zone of the underlying TFZP. It has been found that this factor¹⁰ can effectively

suppress the intensity peaks at the higher-order foci. In principle, none of these factors shows that the use of pinholes is superior to the use of concentric open rings. Therefore, it should be possible to use modulated open rings to construct a large optical element that overcomes the drawbacks of a TFZP.

In this paper we shall theoretically demonstrate this possibility. In particular, we shall propose a modified Fresnel zone plate (MFZP) to produce a sharp Gaussian focal spot. This kind of focal spot is even better than that produced by a photon sieve,⁷ because a focused Gaussian beam has the advantages of circular symmetry, long focal depth, and good beam quality.¹² For simplicity, we shall focus on the case of plane wave illumination.

2. INDIVIDUAL DIFFRACTED FIELDS FROM INDIVIDUAL OPEN RINGS

Consider a MFZP consisting of N concentric open rings. As shown in Fig. 1, it is illuminated by a plane wave. It is suitable to use polar coordinates for those transverse planes that are perpendicular to the common propagation axis. We denote by (r, θ) the polar coordinates at the MFZP plane. Similarly, we denote by (R, ϕ) the polar coordinates at the focal plane. The desired focal point is located at $(R = 0, \phi = 0)$, the focal length is f , and the total radius of the MFZP is A . For convenience, we shall also use the coordinate $s = r^2$ in the remainder of this paper. We denote by $U(R)$ the total diffracted field distribution at the focal plane because it is rotationally symmetric. For the same reason, we denote by $U_n(R)$ the individual diffracted field at the focal plane from the n th individual open ring. According to the linear superposition principle, $U(R)$ is the simple sum of the individual diffracted fields $U_n(R)$ from those individual open rings, i.e., $U(R) = \sum_{n=1}^N U_n(R)$. From the Rayleigh–Sommerfeld diffraction integral,^{13–15} we know that

$$U_n(R) = \frac{1}{\lambda} \int \int_{A_n} \frac{f}{\rho^2} \exp(jk\rho) r dr d\theta, \quad (1)$$

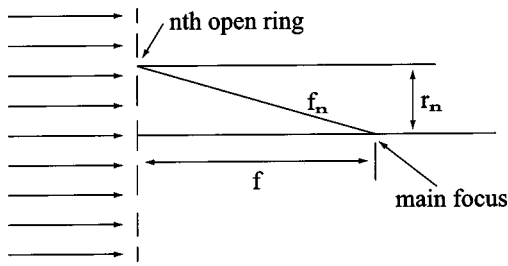


Fig. 1. Schematic view of a modified Fresnel zone plate. See text for the definitions of the parameters f , f_n , and r_n .

where j is the imaginary unit, $k = 2\pi/\lambda$, λ is the wavelength, $\rho = [f^2 + R^2 + r^2 - 2Rr \cos(\theta - \phi)]^{1/2}$, A_n is the area of the n th open ring, and a constant factor $-j$ has been ignored. Equation (1) is accurate provided that¹³⁻¹⁵ $f \gg \lambda$. We now rewrite ρ as $\rho = [f^2 + r_n^2 + R^2 + (r^2 - r_n^2) - 2Rr \cos(\theta - \phi)]^{1/2}$, where r_n is the characteristic coordinate of the n th open ring. For sharp focusing, the area of interest at the focal plane is actually the focal area (i.e., the neighborhood of the focus $R = 0$) because the focal spot is very small. In the focal area, the radial coordinate R is very small. Also, the quantity $r^2 - r_n^2$ is far smaller than the quantity $f^2 + r_n^2$ because the width of the n th open ring is small. By taking these properties into account, we expand ρ as

$$\rho \approx f_n + \frac{R^2 + (r^2 - r_n^2) - 2Rr \cos(\theta - \phi)}{2f_n}, \quad (2)$$

where $f_n = (f^2 + r_n^2)^{1/2}$. This expansion for ρ is similar to that in Eq. (7) of Ref. 15, which studied the off-axis diffraction of circular apertures. We use the approximation of Eq. (2) for the ρ in the exponent of Eq. (1). For the ρ in the denominator of Eq. (1), the approximation $\rho \approx f_n$ is already good enough. By substituting these two approximations into Eq. (1) and using the equality $\int_0^{2\pi} \exp[-ju \cos(\theta - \phi)] d\theta = 2\pi J_0(u)$, where $u = kRr/f_n$, one can obtain

$$U_n(R) = \frac{kf}{f_n^2} \exp\left[jk\left(f_n + \frac{R^2}{2f_n}\right)\right] \times \int_{a_n}^{b_n} \exp\left[jk\frac{r^2 - r_n^2}{2f_n}\right] J_0\left(\frac{kRr}{f_n}\right) r dr, \quad (3)$$

where a_n and b_n are the radii of the lower and the upper edges of the n th open ring, respectively. The integral in Eq. (3) can be re-expressed as $\frac{1}{2} \int_{a_n}^{b_n} \exp[jk(s - s_n)] / (2f_n) J_0(kRs^{1/2}/f_n) ds$ in the s coordinate, where $s_n = r_n^2$. We now let the point $s = s_n$ be the midpoint of the integral interval in the s coordinate. That is to say, we let $a_n^2 = s_n - d_n$ and $b_n^2 = s_n + d_n$, where d_n is the half-width of the n th open ring in the s coordinate. To this end, the geometric structure of the n th open ring can be completely determined by the two parameters s_n and d_n in the s coordinate. As pointed out above, the coordinate R is very small in the focal area. As a consequence, the change of $J_0(kRs^{1/2}/f_n)$ with s is very slow. By taking these factors into account, one can use the approximation $J_0(kRs^{1/2}/f_n) \approx J_0(kRs_n^{1/2}/f_n) = J_0(kRr_n/f_n)$ for the whole but small integral interval $s_n - d_n \leq s \leq s_n$

+ d_n . Then, the factor $J_0(kRr_n/f_n)$ can be put before the integral because it is independent of the integral variable s . The remaining integral $\int_{s_n - d_n}^{s_n + d_n} \exp[jk(s - s_n)] / (2f_n) ds$ can be easily derived to be $4f_n \sin[kd_n/(2f_n)]/k$. By taking all the above analyses into account, we obtain

$$U_n(R) = \frac{2f}{f_n} \exp\left[jk\left(f_n + \frac{R^2}{2f_n}\right)\right] J_0\left(\frac{kr_n}{f_n} R\right) \sin\left(\frac{kd_n}{2f_n}\right). \quad (4)$$

In particular, the field value $U_n(0)$ at the focus $R = 0$ is given by

$$U_n(0) = \frac{2f}{f_n} \exp(jkf_n) \sin\left(\frac{kd_n}{2f_n}\right). \quad (5)$$

To get effective focusing, one should let those individual diffracted fields have the same phase (rigorously speaking, argument) at the desired focus. The argument of the real function $\sin[kd_n/(2f_n)]$ can be 0 or π , because this real function can be positive or negative. By taking this property into account, one can briefly state the general selection condition as follows:

$$f_n = f + m_n \lambda \quad \sin\left(\frac{kd_n}{2f_n}\right) > 0, \quad (6)$$

$$f_n = f + \left(m_n + \frac{1}{2}\right) \lambda \quad \sin\left(\frac{kd_n}{2f_n}\right) < 0, \quad (7)$$

where m_n is a nonnegative integer. Note that the integer m_n is usually different from n . The first relation in Eq. (6) [or Eq. (7)] is used to determine the midpoints of the open rings and the second one to determine their widths. These selection conditions for the open rings of a MFZP are similar to those for the pinholes of a photon sieve.^{7,8,11} In principle, one can get an almost-arbitrarily-small focal spot (up to the order of the wavelength, because evanescent waves cannot reach the focal plane) if the total diameter of the MFZP is large enough. However, one should keep in mind that the efficiency may decrease with the increase of spatial resolution if a certain value for the width of the narrowest open ring is set in advance.

3. CONSTRUCTION OF A GAUSSIAN FOCAL SPOT

It is desirable to produce a Gaussian focal spot because a focused Gaussian beam has the advantages of no side-lobes, circular symmetry, long focal depth, and good beam quality.¹² From the expression $f_n = (f^2 + r_n^2)^{1/2}$, we know that the relative change of f_n with n is small because of the relation $r_n^2 \ll f^2$. Also, R is very small in the focal area. By taking these properties into account, one can get $\exp[jkR^2/(2f_n)] \approx \exp[jkR^2/(2F)]$ and $J_0(kr_n R/f_n) \approx J_0(kr_n R/F)$, where F is the average of all those f_n . The value of F can be approximately given by $F \approx (f_1 + f_N)/2$ if one lets $f_1 < f_2 < \dots < f_N$. Substituting the above approximations into Eq. (4), we get

$$U_n(R) \approx \frac{2f}{f_n} \exp[jk(f_n - f)] \sin\left(\frac{kd_n}{2f_n}\right) J_0\left(\frac{kr_n}{F} R\right). \quad (8)$$

In Eq. (8), we have ignored the factor $\exp\{jk[f + R^2/(2F)]\}$ because it is a common factor for all the open rings and has no influence on the total intensity distribution at the focal plane.

We now divide the whole element into N zones, and let each zone include an open ring. We denote by D_n the width of the n th zone in the s coordinate. Obviously, the sum of those widths D_n is equal to A^2 in the s coordinate. That is to say, $\sum_{n=1}^N D_n = A^2$. We then let

$$\frac{2f}{f_n} \exp[jk(f_n - f)] \sin\left(\frac{kd_n}{2f_n}\right) = \alpha D_n \exp\left(-\frac{s_n}{\sigma^2}\right), \quad (9)$$

where α and σ are two positive-value parameters that can be chosen. It is worth mentioning that Eq. (9) always satisfies the general selection conditions of Eqs. (6) and (7) because its right-hand side is always positive. If all those D_n values are far smaller than A^2 , the approximation $U(R) = \sum_{n=1}^N \alpha D_n \exp(-s_n/\sigma^2) J_0(kR_s^{1/2}/F) \approx \alpha \int_0^{A^2} \exp(-s/\sigma^2) J_0(kRs^{1/2}/F) ds$ holds. Then, if the condition $\exp(-A^2/\sigma^2) \ll 1$ is satisfied, the integral limit A^2 can be replaced by ∞ because the function $\exp(-s/\sigma^2)$ decays very fast with the increase of s . If one further uses the relations

$$s = r^2, \quad ds = 2rdr,$$

$$\begin{aligned} 2\alpha \int_0^\infty \exp(-r^2/\sigma^2) J_0(kRr/F) r dr \\ = \alpha \sigma^2 \exp\{-[\sigma kR/(2F)]^2\}, \end{aligned}$$

one can prove that

$$U(R) \approx \alpha \sigma^2 \exp\left[-\left(\frac{\sigma kR}{2F}\right)^2\right]. \quad (10)$$

Equation (10) explicitly shows that the total diffracted field $U(R)$ at the focal plane is an approximate Gaussian beam with a beam width of $2F/(\sigma k)$. The value $2F/(\sigma k)$ is little larger than the value $2f/(\sigma k)$ because F is little larger than f . By expressing α as $\alpha = 2\beta f \exp(s_1/\sigma^2)/(f_1 D_1)$, one can get the solution

$$d_n = \frac{2f_n}{k} \left\{ L\pi - \arcsin\left[\beta \frac{D_n f_n}{D_1 f_1} \exp\left(-\frac{s_n - s_1}{\sigma^2}\right)\right] \right\}, \quad (11)$$

where L is a positive integer and β is a dimensionless constant. The parameter β must be in the range of $0 < \beta \leq 1$ because it is actually equal to $|\sin[kd_1/(2f_1)]|$. When the selection condition $f_n = f + m_n \lambda$ is used, L should be chosen to be an odd integer. When the selection condition $f_n = f + (m_n + 1/2)\lambda$ is used, L should be chosen to be an even integer. The solution of Eq. (11) has already taken into account the sign problem of the factor $\sin[kd_n/(2f_n)]$ so one does not need to take this sign problem into account any longer. Corresponding to Eq. (11), the full width $2d_n$ falls into the range $(2L - 1)W_n \leq 2d_n \leq 2LW_n$, where $W_n = \lambda f_n$, is the width of the local half-zone of the underlying TFZP⁷ in the s coordinate. After s_n and d_n are determined, the real edges a_n and b_n and the characteristic coordinate r_n of the n th open ring in the r coordinate can be determined by $a_n = (s_n - d_n)^{1/2}$, $b_n = (s_n + d_n)^{1/2}$, and $r_n = s_n^{1/2}$, respec-

tively. It is worth mentioning that the design for any chosen Gaussian focal spot is not unique, because one has many parameters that can be used. However, one should carefully choose the parameters to make the relation $\beta D_n f_n \exp[-(s_n - s_1)/\sigma^2]/(D_1 f_1) \leq 1$ satisfied for each open ring, because Eq. (11) is valid only under this condition. Also, one should ensure the relation $\exp(-A^2/\sigma^2) \ll 1$ is satisfied. Otherwise, the truncation effect may produce sidelobes. Use of the relation $A/\sigma \approx 2$ is suggested.

It can be proven that the peak intensity I_M at the focus is approximately proportional to $4\beta^2 \sigma^4/D_1^2$ for a MFZP. It can also be proven that the intensity I_T at the focus is approximately proportional to $A_T^4/(\lambda^2 f^2)$ for a TFZP, where A_T is the total radius of the TFZP. Therefore, the ratio I_M/I_T is about $4\lambda^2 f^2 \beta^2 \sigma^4/(D_1^2 A_T^4)$. From this relation, one may guess that the intensity I_M at the focus of a MFZP can be higher than the intensity I_T at the focus of a TFZP if the parameter σ is large enough. This guess is indeed correct and will be confirmed by the example presented in Section 4. As we state above, the width of the Gaussian focal spot is about $2f/(\sigma k)$. This relation explicitly shows that one can increase the spatial resolution by increasing the value of σ . Therefore, to get high spatial resolution, one should try to use large σ . However, it should be pointed out that the practical spatial resolution is limited by the errors in fabricating the open rings if the parameter σ is chosen too large.

It is well known that, besides the intensity peak at the principal focus, there also appear significant intensity peaks at the higher-order foci of a TFZP. These higher-order peaks are effectively suppressed by a photon sieve.⁷ It has been found that, for a photon sieve,¹⁰ the suppression of higher orders does not result from the random distribution of pinholes, but from the use of different ratios $d:w$ for different pinholes, where d is the diameter of an individual pinhole and w is the width of the corresponding local half-zone of the underlying TFZP.⁷ In the first-order focus, all the pinholes have constructive contributions to the focusing. However, the sign of an individual diffracted field reverses three times more often in the third-order focus than in the first-order focus. Because the ratios d/w are different for different pinholes, some pinholes still have constructive contributions to the focusing in the third-order focus, but the others have destructive contributions to the focusing in the third-order focus. As a consequence, the total field value at the third-order focus tends to zero and the focusing in the third-order focus is therefore suppressed. The same thing happens in other higher-order foci. According to this explanation, the higher orders of a MFZP can also be effectively suppressed because we actually use different ratios $2d_n/W_n$ for different open rings.

4. NUMERICAL TEST AS EXAMPLE

To understand the above analyses better, we now consider a concrete MFZP. The general parameters for the whole element are chosen such that $\lambda = 2.4$ nm, $f = 500$ μ m, $N = 1015$, $m_N = 4126$, $\sigma = 50$ μ m, $A = 100.032877$ μ m, $F \approx 505$ μ m, $2F/(k\sigma) = 7.715$ nm, and $\beta = 0.96$. The whole element is divided into

Table 1. Related Parameters in the Three Different Regions

Region	n	m_n	f_n	L	D_n
1	$1 \leq n \leq 199$	$2n - 1$	$f + m_n\lambda$	1	$4W_n$
2	$200 \leq n \leq 374$	$396 + 3(n - 199)$	$f + (m_n + 1/2)\lambda$	2	$6W_n^a$
3	$375 \leq n \leq 1015$	$921 + 5(n - 374)$	$f + m_n\lambda$	3	$10W_n$

^a $D_n = 7W_n$ for the 374th open ring.

three regions. In region 1, there are 199 open rings, in region 2, 175 open rings, and in region 3, 641 open rings. The related parameters in these three different regions are presented in Table 1. The width of the narrowest open ring, which is the final one ($n = 199$) in region 1, is 30.02 nm (ideal value). The width of the narrowest opaque ring, which is the outermost one of the whole element, is 24.66 nm (ideal value). The width of the n th opaque ring is given by $a_n - b_{n-1}$ for $2 \leq n \leq 1015$. The width of the first opaque ring is given simply by a_1 because the center is opaque in this example.

Our design considerations (as well as design steps) for this example are as follows:

1. The width of the narrowest open ring is ~ 30 nm because the size of the smallest structure that can be fabricated by lithography^{5,6} is 20–40 nm.

2. The wavelength and the focal distance have the typical values of 2.4 nm and 500 μm , respectively.

3. We let the total radius of the MFZP be ~ 100 μm , as noted. One can find that the width of the outermost half-zone of the underlying TFZP⁷ is ~ 6.12 nm if the total radius of the underlying TFZP is ~ 100 μm . This relation implies that the focal spot size of the MFZP can be as small as 7–8 nm.

4. We let the parameter σ be 50 μm by use of the suggested ratio $A/\sigma \approx 2$.

5. The beam width of the desired Gaussian focal spot is determined to be 7.715 nm.

6. The whole element is divided into three different regions that correspond to $L = 1$, $L = 2$, and $L = 3$, respectively. This separation is necessary; otherwise, one cannot obtain a small focal spot size of ~ 7.7 nm under the condition that the narrowest open ring is ~ 30 nm wide.

7. We let $s_{n+1} - s_n = 6D_n$ in region 2 and $s_{n+1} - s_n = 10D_n$ in region 3. The quantity $s_{n+1} - s_n$ expresses the distance between the midpoint of the n th open ring and the midpoint position of the $(n + 1)$ th open ring in the s coordinate. These choices can ensure that all the opaque rings are wide enough, too.

8. We let $s_{n+1} - s_n = 4D_n$ in region 1. The advantage of this choice is that all the zones (including the first one) in region 1 are symmetric about the corresponding position s_n in the s coordinate.

9. As we point out above, the condition $\beta D_n f_n \exp[-(s_n - s_1)/\sigma^2]/(D_1 f_1) \leq 1$ must be satisfied for each open ring. This condition actually requires that the value $\beta D_n f_n \exp[-(s_n - s_1)/\sigma^2]/(D_1 f_1)$ for the final open ring in region 1 must be smaller than $2/3$. Also, each open ring in region 1 should be wider than 30 nm. We find that these requirements can both be satisfied if the parameter β is not larger than 0.96. Therefore we choose $\beta = 0.96$.

10. Finally, we determine the concrete boundaries of the three regions and choose the detailed parameters for the open rings. These data have been given at the beginning of this section.

To have an intuitive understanding of the layout of this example, in Fig. 2 we draw the transmittance functions in the transition zones between two neighboring regions. One may find that the final zone in region 2 is wider than others in the same region. This arrangement comes purely from the match requirement between region 2 and region 3. As shown in Table 1, we use the relation $f_n = f + (m_n + 0.5)\lambda$ for the open rings in region 2, but use the relation $f_n = f + m_n\lambda$ for the open rings in region 3. Corresponding to these choices, the distance from the midpoint of the final open ring in region 2 to the midpoint of the first open ring in region 3 cannot be an even integral number of W_n . On the other hand, as we state above, we let $s_{n+1} - s_n = 6D_n$ in region 2 and $s_{n+1} - s_n = 10D_n$ in region 3. These choices imply that one can let the width of the final zone in region 2 be $6W_n$ only if the distance from the midpoint of the final open ring in region 2 to the midpoint of the first open ring in region 3 is $8W_n$. However, as we point out above, this condition cannot be satisfied. This being the case, we let the distance from the midpoint of the final open ring in region 2 to the midpoint of the first open ring in region 3 be $9W_n$.

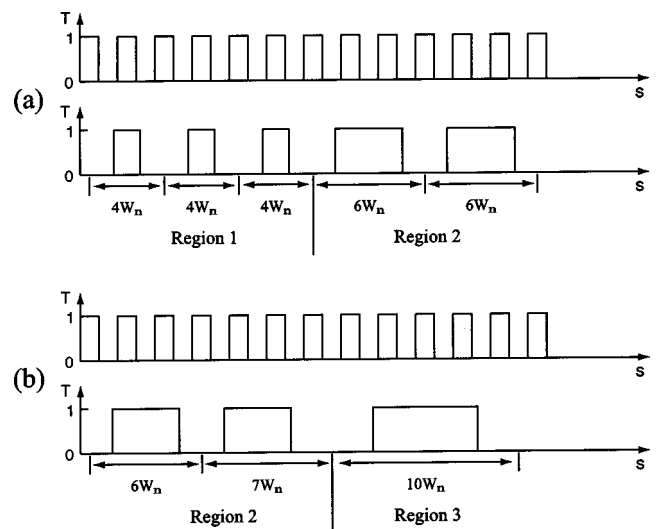


Fig. 2. Transmittance (T) functions of a MFZP (lower graph) and of the underlying TFZP (upper graph) (a) in the transition zones between region 1 and region 2, (b) in the transition zones between region 2 and region 3. For clarity, the widths of all the half-zones of the underlying TFZP are drawn uniformly in the s coordinate.

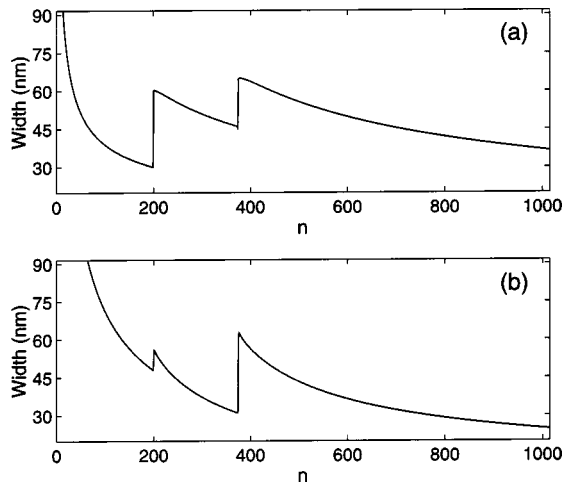


Fig. 3. (a) Change of the widths of the open rings with the increase of n . (b) Change of the widths of the opaque rings with the increase of n .

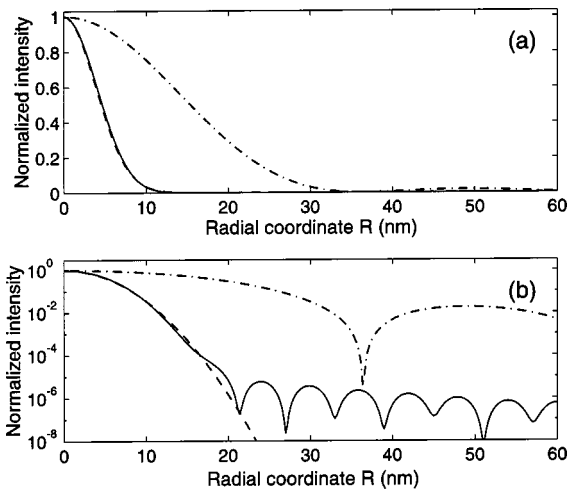


Fig. 4. Normalized intensity distributions (to the peak intensity in each case) at the focal plane for an ideal MFZP and for the corresponding TFZP: (a) linear plots, (b) logarithmic plots. The solid curves are the intensity distributions of the ideal MFZP, the dashed curves are the desirable Gaussian distributions, and the dashed-dotted curves are the intensity distributions of the TFZP.

Corresponding to this distance, we let the width of the final zone in region 2 be $7W_n$.

To further understand the layout of this example, we draw the real widths of the open rings as a function of n in Fig. 3(a). Basically, the widths of the open rings decrease with the increase of n in each region but have abrupt jumps at the boundaries between two neighboring regions. These jumps are related to the abrupt jumps of L and D_n . For completeness, the change of the real widths of the opaque rings with the increase of n is shown in Fig. 3(b).

The calculated intensity distributions at the focal plane for this ideal MFZP and for an opaque-center TFZP are presented in Fig. 4. These simulations are based on the Rayleigh–Sommerfeld diffraction integral.^{13–15} For the TFZP, the width of the outermost open ring is 29.94 nm, the total radius A_T is 20.084 μm , the focal length f is 500 μm , and the wavelength λ is 2.4 nm. From Fig. 4, one can see the following properties: (1) As shown in Fig.

4(a), the intensity distribution of the ideal MFZP is in excellent agreement with the desirable Gaussian intensity distribution with a beam width of 7.715 nm. (2) As shown in Fig. 4(a), the focal spot size of the ideal MFZP is much smaller than that of the TFZP. (3) As shown in Fig. 4(b), the sidelobes of the intensity distribution of the ideal MFZP have been effectively suppressed. The calculated intensity distributions on the propagation axis for this ideal MFZP and for the corresponding TFZP are shown in Fig. 5. These simulations are also based on the Rayleigh–Sommerfeld diffraction integral.^{13–15} For the calculations of the on-axis intensity distributions, one only needs to replace the focal length f by the axial distance Z . We define the axial distance Z as the distance between the central point of the MFZP (or the TFZP) and the on-axis observation point. From Fig. 5 one can see that the higher orders of the ideal MFZP have been effectively suppressed, although there appear several small intensity peaks at other axial locations. This suppression directly confirms the opinion of Ref. 10, because the ideal MFZP is a rotationally symmetric element. In addition, we find that the calculated peak intensity I_M of the ideal MFZP is 8.57 times higher than the peak intensity I_T of the TFZP. On the other hand, the ratio I_M/I_T determined by the approximate formula $I_M/I_T \approx 4\lambda^2 f^2 \beta^2 \sigma^4 / (D_1^2 A_T^4)$ is 8.85. These two values are in good agreement.

As we point out above, the errors in fabricating the open rings may have an important influence on the practical spatial resolution if the parameter σ is chosen to be large. To see if this inaccuracy has a significant influence on the performance of the above-mentioned example, we numerically introduce random errors into the edge parameters of the open rings. Concretely, for each open ring we put two different random errors on the ideal edge values, respectively. All random errors are distributed in the range of $[-2 \text{ nm}, +2 \text{ nm}]$. That is, we assume that the accuracy for the edge values of those open rings is $\pm 2 \text{ nm}$. We did many numerical experiments. Each time, we found that the normalized intensity distribution at the focal plane for the nonideal MFZP with errors is almost indistinguishable from that for the ideal MFZP in the lin-

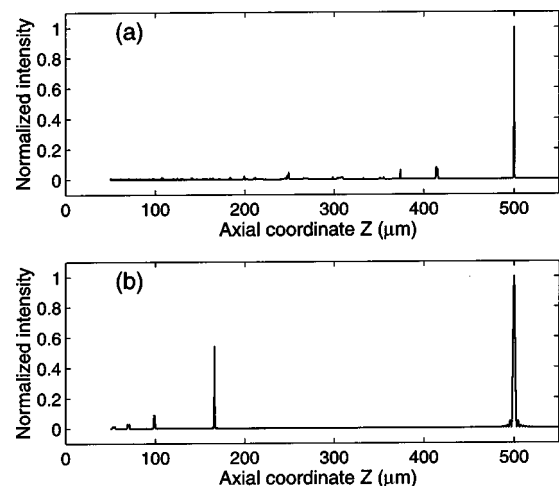


Fig. 5. Normalized intensity distributions (to the peak intensity in each case) on the propagation axis: (a) the ideal MFZP, (b) the corresponding TFZP.

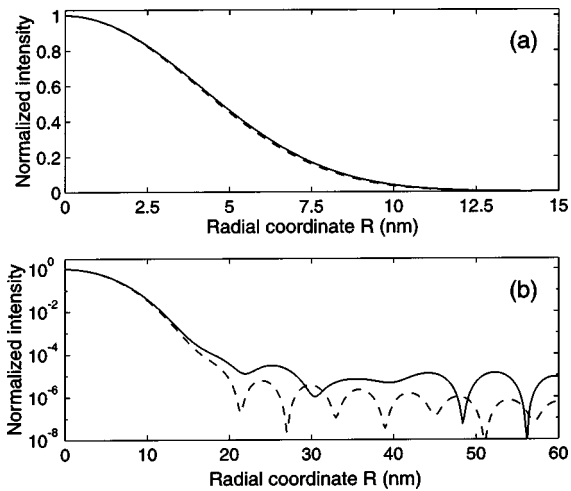


Fig. 6. Normalized intensity distributions (to the peak intensity in each case) at the focal plane for a nonideal MFZP with errors: (a) linear plots, (b) logarithmic plots. The solid curves are the intensity distributions of the nonideal MFZP with errors, and the dashed curves are the intensity distributions of the ideal MFZP.

ear scale. One of these simulations is shown in Fig. 6. These numerical experiments show that the accuracy of ± 2 nm is sufficient for the example chosen.

5. CONCLUSIONS

We have proposed a MFZP that can produce a sharp, Gaussian focal spot for the focusing and imaging of soft x rays and extreme ultraviolet radiation. The focal spot size can be much smaller than the minimum structure size of the diffractive optical element, and the sidelobes and the higher orders can be effectively suppressed. Through a concrete example, we have numerically confirmed these properties. In particular, we have shown that a Gaussian focal spot with a beam width of 7.7 nm can be produced by a MFZP with a minimum structure size of 30 nm. A MFZP can be fabricated by the same technology as for a TFZP. Compared with a photon sieve,⁷ a MFZP has the advantages of circular symmetry, long focal depth and good beam quality.¹² Its disadvantages are the additional small intensity peaks on the propagation axis and the need for additional support.

Qing Cao, the corresponding author, may be reached by e-mail at qing.cao@fernuni-hagen.de.

REFERENCES AND NOTES

1. G. Schmahl, D. Rudolph, P. Guttman, and O. Christ, "Zone plates for x-ray microscopy," in *X-Ray Microscopy*, G. Schmahl and D. Rudolph, eds. (Springer-Verlag, Berlin, 1984), Vol. 43, pp. 63–74.
2. H. Arsenault, "Diffraction theory of Fresnel zone plates," *J. Opt. Soc. Am.* **58**, 1536 (1968).
3. D. J. Stigiani, R. Mittra, and R. G. Semonin, "Resolving power of a zone plate," *J. Opt. Soc. Am.* **57**, 610–613 (1967).
4. J. A. Sun and A. Cai, "Archaic focusing properties of Fresnel zone plates," *J. Opt. Soc. Am. A* **8**, 33–35 (1991).
5. E. H. Anderson, V. Boegli, and L. P. Murray, "Electron beam lithography digital pattern generator and electronics for generalized curvilinear structures," *J. Vac. Sci. Technol. B* **13**, 2529–2534 (1995).
6. E. H. Anderson, D. L. Olynick, B. Harteneck, E. Veklerov, G. Denbeaux, W. Chao, A. Lucero, L. Johnson, and D. Attwood, "Nanofabrication and diffractive optics for high-resolution x-ray applications," *J. Vac. Sci. Technol. B* **18**, 2970–2975 (2000).
7. L. Kipp, M. Skibowski, R. L. Johnson, R. Berndt, R. Adlung, S. Harm, and R. Seemann, "Sharper images by focusing soft X-rays with photon sieves," *Nature* **414**, 184–188 (2001).
8. Q. Cao and J. Jahns, "Focusing analysis of the pinhole photon sieve: individual far-field model," *J. Opt. Soc. Am. A* **19**, 2387–2393 (2002).
9. G. E. Artzner, J. P. Delaboudinière, and X. Y. Song, "Photon sieves as EUV telescopes for solar orbiter," in *Innovative Telescopes and Instrumentation for Solar Astrophysics*, S. L. Keil, S. V. Avakyan, and S. I. Vavilov, eds., Proc. SPIE **4853**, 158–161 (2003).
10. M. Howells, <http://www-esg.lbl.gov/esg/personnel/howells/Xraysieves.pdf>. The opinion that the suppression of higher orders results not from the random distribution of pinholes but from the use of different ratios d/w for different pinholes is presented in this reference, where d is the diameter of an individual pinhole and w is the width of the corresponding local half-zone of the underlying TFZP.
11. Q. Cao and J. Jahns, "Nonparaxial model for the focusing of high-numerical-aperture photon sieves," *J. Opt. Soc. Am. A* **20**, 1005–1012 (2003).
12. A. E. Siegman, "New developments in laser resonators," in *Optical Resonators*, D. A. Holmes, ed., Proc. SPIE **1224**, 2–14 (1990).
13. J. E. Harvey, "Fourier treatment of near-field scalar diffraction theory," *Am. J. Phys.* **47**, 974–980 (1979).
14. W. H. Southwell, "Validity of the Fresnel approximation in the near field," *J. Opt. Soc. Am.* **71**, 7–14 (1981).
15. C. J. R. Sheppard and M. Hrynevych, "Diffraction by a circular aperture: a generalization of Fresnel diffraction theory," *J. Opt. Soc. Am. A* **9**, 274–281 (1992).